Letters in High Energy Physics Volume 2024
ISSN: 2632-2714

Received: 13.05.2024 Accepted: 26.07.2024 Published: 19.08.2024

Integrity Assessment of Pipelines Containing Circumferentially Oriented Surface Defects

Belkacemi Mohamed Hicham[a], Benzerga Djebbara[a*], Chouiter Adel [b], Haddi Abdelkader[c]

[a]LSCMI, University of Sciences and Technology of Oran, Mechanical Department, 31000, Oran, Algeria.
belkacemimh@gmail.com https://orcid.org/0009-0007-8117-8706
djebbara.benzerga@univ-usto.dz https://orcid.org/0000-0003-2238-6488
[b]University Frères Mentouri Constantine 1, 25000, Algeria.
adel.chouiter@umc.edu.dz https://orcid.org/0009-0003-1064-1805
[c]Univ. Artois, IMT Lille Douai, Junia, Univ. Lille, ULR 4515, Laboratoire de Génie Civil et géo Environnement (LGCgE), 62400, Béthune, France.
Abdelkader.haddi @univ-artois.fr https://orcid.org/0000-0003-3675-1570

ABSTRACT

The main external defects on pipelines can be introduced during handling, welding and during service by the aggressiveness of the soil. Mechanical damage scratches occur during handling, storage, laying, backfill, rip rap dumping, etc. ll these defects present on the external surface of the pipe, significantly reduce its strength and constitute potential sources of damage. The hydrostatic test has little value for circumferential defects; the main stress is in the direction of the hoop and has little significance for defects. Therefore, the hydrostatic test is not a test for defects located on the circumference of the pipe. This approach will address the weaknesses of the hydrostatic test when assessing the structural integrity of pipes with circumferential surface defects using non-destructive examination (NDT) in-depth and a numerical simulation before the commissioning of the defective pipe.

Keywords: Structural integrity assessment; pipeline; circumferential surface defect; damage, numerical simulation

1. Introduction

Pipelines are used worldwide to transport gas and oil as well as other fluids such as hydrogen are undoubtedly the safest way to transport such products. Subject to damage from handling, corrosion, and welding, pipelines must be inspected regularly to ensure their structural integrity and compliance with regulations, as well as to assess their remaining useful life [1]. The spiral welded pipe is fundamental to this transportation system and has become highly sought after in the market. The production of pipes made from micro-alloyed steels has seen significant growth to meet operational requirements, which have been further pushed to even higher limits in terms of pressure, flow rate, lengths, and thickness [2]. However, whether during their manufacturing or while being used, defects can show up on their outer surface, which could potentially cause damage [3]. Near the defects, high stress concentrations cause significant plastic deformations that can lead to the formation of cracks resulting in pipe failure [4]. Control technologies offer several options in the field of Non-Destructive Testing for pipeline inspection; no method can do everything during an inspection [5]. According to the specific data collection needs, one can choose one or more pipeline inspection solutions. The integrity of the pipelines depends on the integrity of its inspection equipment [6]. Proven solutions from Control Technologies need to provide accurate, reliable, and reproducible real-time data. In-service inspections promote time and cost savings, ensure environmental and human safety, and confirm the long-term reliable performance of pipeline infrastructure [7].

Superficial corrosion defects can be detected by smart devices such as Emersion detection devices that can constantly collect data and identify weak points in a pipeline [8]. For welding defects, industrial radiography remains the most commonly used non-destructive testing (NDT) method for inspecting gas pipeline welds [9]. A new automated vision system has just been introduced for detecting and evaluating welding defects in gas pipelines from radiographic films [10]. This vision system uses image captures for radiographic films and applies image processing and computer vision algorithms to detect welding defects and allows the evaluation of very useful information such as the length, width, area, and perimeter of defects [11]. Superficial scratches are considered as cracks with a larger width. Evaluating their dimensions can be done in the same way as corrosion defects. The focus of this article is on evaluating the structural integrity of a pipe in the presence of a circumferential surface defect, allowing for the determination of the size of the critical defect when the pipe is subjected to operating pressure and hydrostatic testing. This procedure will help address the weaknesses of the hydrostatic test when evaluating external defects located on the circumference of the pipe. The hydrostatic test has little value for evaluating circumferential defects. The main tangential stress which is the most important stress, is not very important for these defects, as it tends to cause inactive damage by closing the defect.

2. Mechanical model

The circumferential surface defect present on the tube is shown in Figure 1. The defect is represented by a number of dimensionless parameters including the relative depth (d/t), relative thickness (t/R), and the appearance ratio (d/b). The length of the defect l is measured along the circumference of the pipe. The simulation of the pipe with the defect is conducted using the ANSYS code and the APDL language. Due to the symmetry of the structure, a half cylinder is discretized to save on calculation time [12, 13]. By entering data like material properties, pipe geometry, and internal pressure, the code calculates the necessary physical quantities.

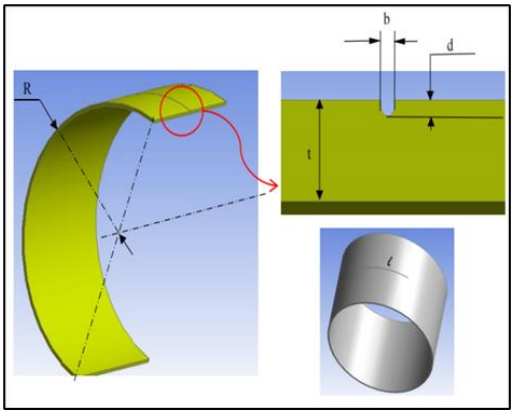

Figure 1. Scheme illustrating the outer surface of the pipe and the dimensions of defects.

In this study, the surface defect of the pipe in the tangential direction is examined. The propagation of the defect is caused solely by the main axial stress, which is half of the main hoop stress. That's why a crack initiated at the defect level propagates in the tangential direction of the pipe. The damage is considered very localized near the superficial defect, where plastic deformations are significant, leading to material degradation in a small volume [14]. We consider that failure occurs when the damage value reaches the critical damage value of the material Dc. The steel grade used is micro-alloyed steel used for manufacturing API X65 pipelines. Table 1 summarizes the mechanical properties of the material [15].

Table 1. Mechanical properties of API 5L X65 steel [15].

E, Young modulus (GPa)	**υ, Poisson ratio**	**σ_y, Yield strength (MPa)**	**σ_u, ultimate strength (MPa)**	**σ_u, true ultimate strength (MPa**
210	0.3	464	563	629

Figure 2 represents the tensile curve of API X65 materials [15]. This curve will be implemented in the ANSYS code for determining the critical dimensions of the surface defect.

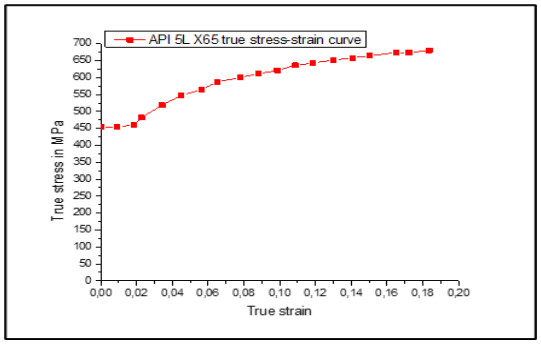

Figure 2. True tensile curve of API 5L X65 steel [15].

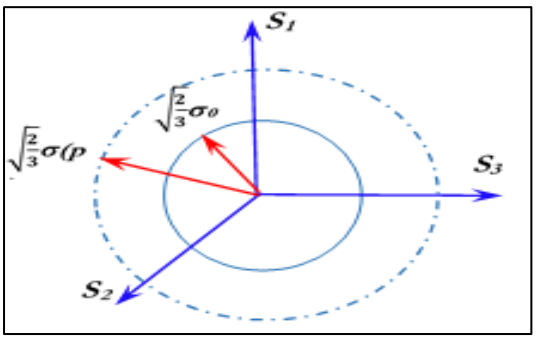

Figure 3. Expansion of the Von Mises elasticity domain: isotropic hardening.

It is assumed here that the material undergoes isotropic hardening taking into account the expansion of the elastic domain with plastic deformation (Figure 3). It is assumed that the plastic yield function can be expressed as follows:

$$f = (\sigma, p) = \sigma_{eq} - \sigma(p) \quad (1)$$

σ_{eq} is the Von Mises stress: $\sigma_{eq}\left(\frac{3}{2} s_{ij}s_{ij}\right)^{1/2}$

$\boldsymbol{s} = \sigma - \frac{1}{3}(tr\sigma)1$ is the stress deviator and $\sigma(p)$ is a function that increases with the cumulative equivalent plastic strain, defined as:

$$p = \int_0^t \dot{p}(\tau)\, d\tau \; ; \; \dot{p} = \left(\frac{2}{3}\dot{\varepsilon}^p : \dot{\varepsilon}^p\right)^{1/2} \quad (2)$$

The function $\sigma(p)$ is known experimentally. This scalar function is required to be equal to the initial yield stress σ_0 when the cumulative equivalent plastic strain is zero.
$\sigma(p = 0) = \sigma_0$.

We write the function $\sigma(p)$ like a power law, which is the Ramberg-Osgood law $\sigma(p) = \sigma_0 + Kp^n$ where K and n are material coefficients. We assume in the case of small deformations an additive partition of the total deformation into elastic and plastic parts for the three-dimensional case similar to the one-dimensional observation:

$$\varepsilon = \varepsilon^e + \varepsilon^p \quad (3)$$

Plastic flow can only occur if the stress state representative point σ reaches the yield surface and remains there; such that the point cannot leave the surface ($f > 0$ is impossible).

For modeling the progressive damage evolution of the material until the initiation of a mesoscale crack, we use damage mechanics. An isotropic damage variable is introduced as an internal variable [16]:

$$D = \frac{\delta S_D}{\delta S} \; ; 0 \le D \le D_c \quad (4)$$

Where $\boldsymbol{\delta S}$ represents the total damaged surface of the representative elemental volume, while $\boldsymbol{\delta S_D}$ represents the equivalent surface area of microcracks within. Dc is the critical value of damage that depends on the material and temperature. By introducing the concept of effective stress [17], equation (1) can be written in this case as:

$$f(\sigma, p) = \tilde{\sigma}_{eq} - \sigma(p); with\ \tilde{\sigma}_{eq} = \frac{\sigma_{eq}}{1 - D} \quad (5)$$

The rate of plastic deformation $\dot{\varepsilon^p}$ is normal to the yield surface. This is the normality law, which is expressed by the following equation:

$$\dot{\varepsilon^p} = \dot{\lambda}\frac{\partial f}{\partial \sigma} \quad ; \quad \dot{\lambda} \geq 0 \tag{6}$$

$$\dot{\varepsilon^p} = \dot{\lambda}\frac{\partial f}{\partial \sigma} = \frac{3}{2}\frac{s}{\sigma_{eq}}\frac{\dot{\lambda}}{1-D} \quad ; \quad if \begin{cases} f = 0 \\ \dot{f} = 0 \end{cases} \tag{7}$$

$\boldsymbol{s}$ Represents the stress deviator and $\dot{\lambda}$ is called the plastic multiplier, which is positive or zero.

It is possible to show that $\dot{\lambda} = \dot{p}$

The evolution law of damage, valid for ductile damage, is derived from the dissipation potential [18]:

$$F = f + F_D \tag{8}$$

The damage evolution law is given by

$$\dot{D} = \dot{\lambda}\frac{\delta F}{\delta Y} = \dot{\lambda}\frac{\delta F_D}{\delta Y} \quad ; \quad F_D = \frac{S}{(s+1)(1-D)}\left(\frac{y}{S}\right)^{s+1} \tag{9}$$

S And s are two material- and temperature-dependent parameters and Y is the associated variable to D defined by [19]:

$$Y = \frac{\check{\sigma}_{eq}^2 R_v}{2E}$$
$$R_v = \frac{2}{3}(1+v) + (1-2v)\left(\frac{\sigma_H}{\sigma_{eq}}\right)^2 \tag{10}$$

Rv is the triaxiality function. The relation (9) becomes:

$$\dot{D} = \left(\frac{Y}{S}\right)^s \dot{p} \quad ; if \quad p \geq p_0 \tag{11}$$

A subroutine written in ANSYS APDL language has been integrated into the main code. The finite element analysis code aims to identify the critical point C^* where significant plasticized zones are present due to the ductility of material API X65. These plastic deformations may be associated with micro cracks. At the critical point C*, the finite element analysis calculation allows us to obtain the following physical quantities:
$\varepsilon_{ij}(C^*,t), \varepsilon_{ij}^e(C^*,t), \varepsilon_{ij}^p(C^*,t), \sigma_{ij}(C^*,t)$

The length of the defect is set to a given value. For each length of the defect, the depth is initialized at the beginning of the calculation to a very low value ($d0$) so that the behavior at point C^* remains elastic at the beginning of the depth increment. The yield function f at this point is strictly negative (see equation 1). Then the depth is gradually incremented $d(t_{n+1}) = d(t_n) + \Delta d$ until the appearance of plastic deformations. When the load function f is strictly positive ($f > 0$ is impossible) for a given value of the defect depth. In this case, a plastic correction is necessary according to a return mapping algorithm based on an elastic prediction and then a plastic correction, which exploits the separation of the elastic-plastic operator [20], as explained below to find the plastic solution.

The relations (5-12) are discretized in an incremental form corresponding to a fully implicit integration scheme which has the advantage of being unconditionally stable [21-22]. We then carry out a plastic correction step in which the objective is to calculate the solution Δp and $\Delta\check{\sigma}$ which makes it possible to determine p and $\check{\sigma}$. The plastic deformation ε^p and the damage D are calculated from the discretized relationships and finally the stresses are obtained from $\sigma^{\check{}} = \sigma/1 - D$. Algorithm below summarizes the implementation of the radial return method (return mapping). For a value of the defect depth d_{n+1} and when $f > 0$, the solution must satisfy the following relationships:

$$f = \check{\sigma}_{eq} - \sigma_s = 0, \ \check{\sigma} = \lambda tr\varepsilon 1 + 2\mu\left(\varepsilon - \varepsilon_n^p - \Delta\varepsilon^p\right)$$
$$\Delta\varepsilon^p = \Theta\Delta p, \ \Delta D = \left(\frac{Y}{S}\right)^s \Delta p \tag{12}$$

With:

$$\Delta(x) = (x)_{n+1} - (x)_n \ \text{ And } \Theta = \frac{3}{2}\left(\frac{\check{s}}{\check{\sigma}_{eq}}\right)$$

By replacing $\Delta\varepsilon^p$ with its expression, the problem is reduced to a system with two unknowns:

$$f = \breve{\sigma}_{eq} - \sigma_s = 0$$
$$\mathcal{g} = \breve{\sigma} - \lambda tr\varepsilon 1 - 2\mu\left(\varepsilon - \varepsilon_n^p\right) + 2\mu\Theta\Delta p \quad (13)$$

Newton implicit iterative method greatly simplifies the construction of the solution of this system and is only valid with the Von Mises criterion and an implicit discretization. At each iteration (i), we have

$$f + \frac{\partial f}{\partial \breve{\sigma}} : \Xi_{\breve{\sigma}} = 0,$$
$$\mathcal{g} + \frac{\partial \mathcal{g}}{\partial \breve{\sigma}} : \Xi_{\breve{\sigma}} + \frac{\partial \mathcal{g}}{\partial p}\Phi_p = 0 \quad (14)$$

With

$$\Xi_{\breve{\sigma}} = (\breve{\sigma})_{i+1} - (\breve{\sigma})_i \ , \Phi_p = (p)_{i+1} - (p)_i$$

Which define the corrections.

The functions f and g as well as their partial derivatives are considered at iteration t_{n+1} (for a given value of depth) and at iteration (i). When the damage is determined, it is compared to its critical value D_c. If this value is reached, the subroutine will display the critical size of the defect (see figure 4).

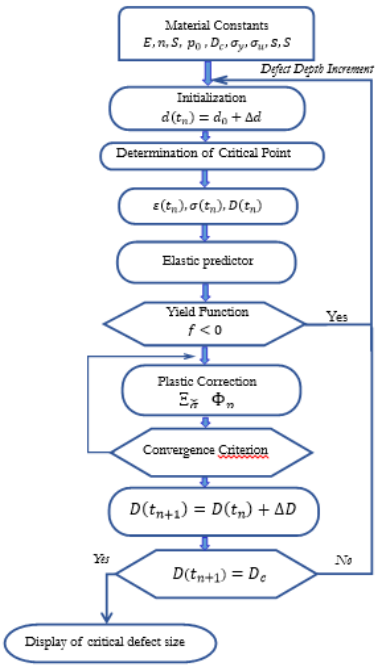

Figure 4. Flowchart for determining the critical defect.

3. NUMERICAL SIMULATION

The simulation was conducted using the APDL language of the ANSYS code. For the mesh of the structure we used quadratic elements which are best suited for simulations aimed at determining a stress (or a deformation) in a zone with strong gradients, such as a zone of stress concentration, here the surface defect (22). A more refined mesh was used at the defect level (figure 5). For each defect length, we will determine the depth at which the damage reaches the critical value Dc at critical point C* where plastic deformations are maximal (figure 6). The width of the defects was set at 5 mm (see figure 7). It is assumed that the width of the defect has little effect. In fact, figure 5 shows that changing the width of the defect doesn't have much of an effect on the maximum Von Mises stress or the maximum plastic deformations at the bottom of the defect. This simulation is initially performed for a pressure equal to the operating pressure (71 bars) and then for a pressure equal to the hydrostatic test pressure (1.5 times the operating pressure). The pre-service hydrostatic test is used to prove the integrity of a pipeline before it is put into service. The hydraulic test pressure is always higher than the design pressure, providing a safety margin against design tolerance and defect growth during pipeline service. The objective of this simulation campaign is to determine the effect of the test pressure on the removal of defects of a given depth and length, aiming to find an alternative solution to the hydrostatic test, the disadvantages of which were mentioned in the introduction. The selected project for this study is the GZ1 40" pipeline connecting the southern Algerian production region of Hassi R'mel to the northern region of Arzew for operation. The pipe has an API X 65 grades, with a diameter of 1016 mm and a thickness of 12.7 mm. In the first stage, the simulation involves determining the critical defect size for a pressure equal to the operating pressure, which will allow plotting the curve highlighting the region where defects can survive and those that will not survive at this pressure. In the second stage, the same work is carried out for a pressure equal to 1.5 times the operating pressure, which will result in obtaining the hydrostatic test curve that delineates the safety region and the dangerous region (see figure 8).

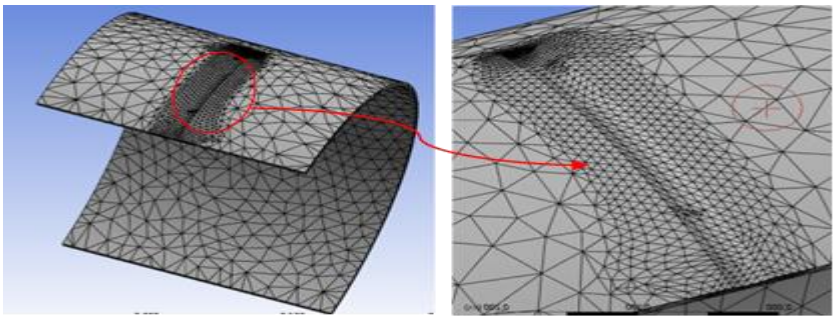

Figure 5. Finite Element Model pipe with external defect.

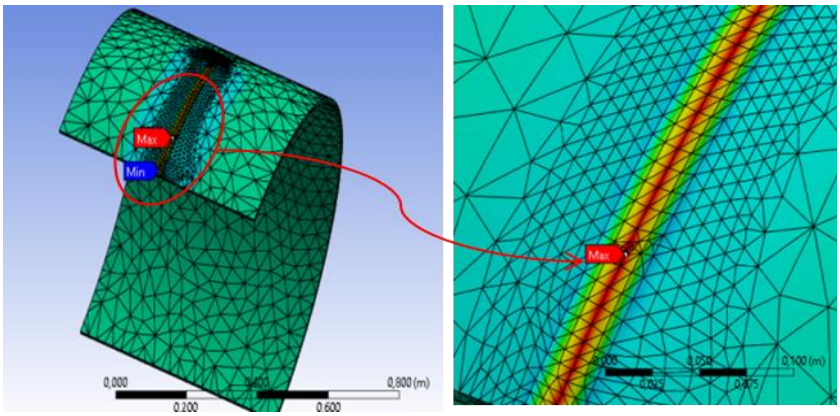

Figure 6. Critical zone where plastic deformations are maximum.

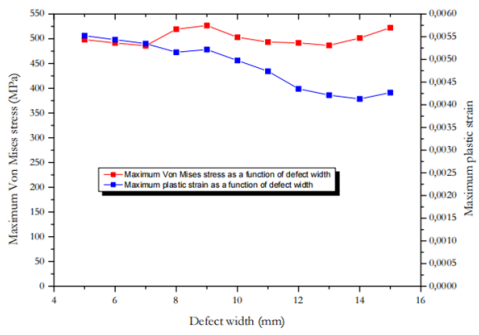

Figure 7. Effect of the defect width on the maximum Von Mises stress and maximum plastic deformation.

Figure 8 highlights the different defect zones according to their sizes. Defects circumscribed in the class 3 zone are distinguished by large dimensions and fail at the operating pressure and consequently at the hydrostatic pressure. These defects will require repair depending on the nature of the defect. In the case of a corrosion defect or defect in the form of a scratch, the repair can be carried out using a "clock spring" composite system. In the case of a welding defect, gutters or cracks, the weld must be repaired by removing it and carrying out a new weld (successive repairs). Class 2 represents defects that resist working pressure but not hydrostatic pressure. Pipes with such defects cannot be accepted since they contain defects that have failed the hydrostatic test. This zone represents a safety margin since defects that survive the hydrostatic test can withstand the operating pressure. Class 1 defects have smaller dimensions, can therefore survive the hydrostatic test and pose no danger to the pipe, in this case defects whose depth is less than 10% of the thickness of the pipe. In this zone the pipe remains insensitive to the size of the defects. To illustrate the evolution of the damage as a function of the depth of the defect and the internal pressure, several defects were selected to be exposed to the operating pressure (71 bars) then to the hydrostatic test pressure (1.5 times the operating pressure) (see table 2). Each defect, with its extension, was subjected to both pressures. The objective is to demonstrate the evolution of the damage as a function of the pressure and the size of the defect. The width was maintained at 5 mm and the critical damage of the material $D_c = 0.85$.

Table 2. Surface circumferential defects retained.

[ZnAc] (M)	Defect length (mm)	Pressure
Def_1	88	Operating
Def_2	307.6	Operating
Def_3	560	Operating
Def_4	88	Hydrotest
Def_5	307.6	Hydrotest
Def_6	560	Hydrotest

To confirm the results shown in Figure 9, we used the ASME/B31G standard [23], widely accepted for rehabilitating corroded pipelines and supported by experiments. This standard helped calculate the normalized defect lengths $(L/R*t)$^0.5 for various normalized relative depths (d/t) (see Figure 9). This method confirmed the conclusions obtained through the approach developed within the scope of this article. The results obtained using the approach developed in this work are very close to those obtained by the modified B31G.

La figure 10 illustrates that under high pressure and substantial extension of the defect, the material damage advances quickly until it reaches its critical value, resulting in the rupture of the material. In Figure 10, we can see that the damage threshold starts at a depth of 10% of the pipe thickness, matching well with the threshold predicted by the B31G standard, which suggests that beyond this threshold, an external defect on a pipe becomes dangerous.

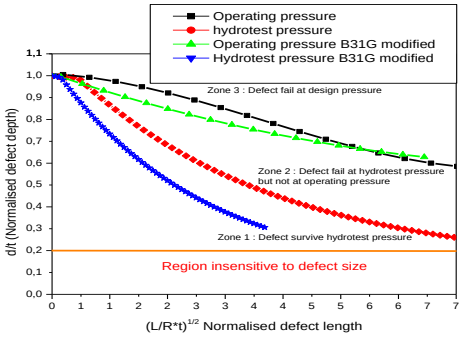

Figure 8. The impact of testing pressure on eliminating critical depth and length defects.

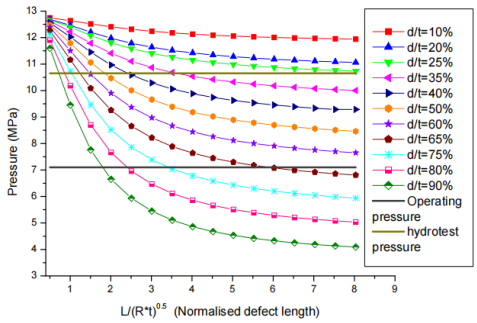

Figure 9. B31G modified norme for results validation.

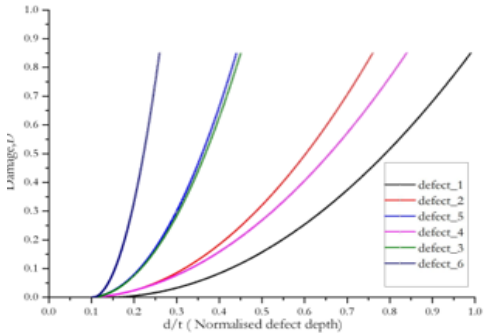

Figure 10. Damage evolution curves depending on the pressure and the depth for different lengths of defects.

4. CONCLUSION

Surface circumferential defects resulting from on-site circumferential welding, corrosion, or handling can be a cause for concern because hydrostatic testing has little value for these defects. The maximum principal stress, which is the tangential stress, is of little importance for these defects. Therefore, the hydro test is not a test to detect defects located on the circumference of the pipe. This article presents an approach to determine the critical size of the surface defect when the pipe is subjected to the operating pressure or the hydrostatic test pressure. This approach combines in-depth non-destructive testing (NDT) and numerical simulation before putting a pipe with a circumferential surface defect into service. Based on the continuum damage mechanics, the method has allowed determining the critical defect size corresponding to the critical damage value. This will enable the assessment of the threat posed by a circumferential surface defect on a pipe before it is put into service. This method could provide high-quality results and compensate for all the benefits

resulting from conducting a hydrostatic test for an axial surface defect. This would involve the development of more advanced behavior and damage laws that would ensure the same level of integrity as that provided by the hydrostatic test.

References

[1] J. Vincent-Genod, Le transport des hydrocarbures liquides et gazeux par canalisation. Institut français de pétrole. Société des éditions technique, Paris (1989).

[2] B. Kerboua, Étude de la dégradation d'un cordon de soudure d'un acier API X70. Edition universitaire européenne, (2021).

[3] S. Sainson, Inspection en ligne des pipelines. Principes et méthodes par Éditions Tec & Doc – Lavoisier, (2007), ISBN : 978-2-7430-0972-4.

[4] M. Allouti, Étude de la nocivité de défauts dans les canalisations de transport de gaz tels les éraflures, les enfoncements ou leurs combinaisons. Thèse de doctorat, Université Paul Verlaine de Metz (2010).

[5] C. Fouquet, Aide à la détection et à la reconnaissance de défauts structurels dans les pipelines par analyse automatique des images XtraSonic. Thèse de doctorat, Université de Cergy-Pontoise - Ecole doctorale Sciences et Ingénierie (2015).

[6] TECHNOLOGIE SKIPPER NDT. Inspection des pipes non raclables. Société skipper NDT (2015).

[7] Y. Sahraoui, Optimisation des méthodes d'inspection des pipes. Thèse de doctorat soutenue (2014), université Annaba.

[8] J. A. Beavers and N. G. Thompson, External Corrosion of Oil and Natural Gas Pipelines. ASM Handbook (2006), Volume 13C, Corrosion: Environments and Industries.

[9] O. Marlier-Viard, G. Delattre, F. Leroux, Filmless radiography: an innovative application to guarantee pipelines quality. EUROPIPE France (2004).

[10] I. M. Elewa, E. Gadelmawla, H. Shafeek, Assessment of welding defects for gas pipeline radiographs using computer vision, Third Assiut University Int. Conf. On Mech. Eng. Advanced Tech. For Indus. Prod. December, 24-26 (2002).

[11] H. Shafeek, E. Gadelmawla, A. Abdel-Shafy, and I. Elewa, Assessment of welding defects for gas pipeline radiographs using computer vision, NDT & e International, 4, 291-299 (2004).

[12] A. Regad, D. Benzerga, H. Berrekia, A. Haddi, and N. Chekhar, Repair and rehabilitation of corroded hdpe100 pipe using a new hybrid composite, Frattura ed Integrità Strutturale, 56, 115-122 (2021).

[13] H. Berrekia, D. Benzerga, and A. Haddi, Behavior and damage of a pipe in the presence of a corrosion defect depth of 10% of its thickness and highlighting the weaknesses of the asme/b31g method, Frattura ed Integrità Strutturale, 49, 643-654 (2019).

[14] D. Benzerga, Burst pressure estimation of corroded pipeline using damage mechanics. in Conference on Multiphysics Modelling and Simulation for Systems Design. Springer, 481-488 (2014).

[15] H.S. Darwish Talouti, D. Benzerga, A. Haddi, Numerical Investigations of Damage Behaviour at the Weld/Base Metal Interface. , IJE TRANSACTIONS C: Aspects, 12, 2337-2343 (2022).

[16] J. Lemaitre, Model for Ductile Fracture, Journal of Engineering Materials and Technology, 107/83 (1985).

[17] M. Nadjafi, P. Gholami, Reliability Analysis of Notched Plates under Anisotropic Damage Based on Uniaxial Loading using Continuum Damage Mechanics Approach, IJE TRANSACTIONS A: Basics, 01, 253-262 (January 2021).

[18] J. Lemaitre, R. Desmorat, Isotropic and Anisotropic Damage Law of Evolution. Handbook of Materials Behavior Models, 0-12-443341-3 (2001).

[19] P. Gholami, M. A. Kouchakzadeh, M. A. Farsi, A Continuum Damage Mechanics-based Piecewise Fatigue Damage Model for Fatigue Life Prediction of Fiber-reinforced Laminated Composites.IJE TRANSACTIONS C: Aspects, 6, 1514-1525 (June 2021).

[20] T. Heuzé, Plasticité des structures, École d'ingénieur, Ecole Centrale de Nantes, France.cel-02059317 (2015).